PATH-DEPENDENT MORPHOLOGICAL EVOLUTION OF SE-TE MESOSTRUCTURES PREPARED BY INORGANIC PHOTOTROPIC GROWTH

KATHRYN R. HAMANN[†], AZHAR I. CARIM[†], MADELINE C. MEIER[†], NATHAN S. LEWIS[†,*]

[†]Division of Chemistry and Chemical Engineering
California Institute of Technology
Pasadena, CA 91125

ABSTRACT

We describe herein a path dependent "history" effect wherein the film morphology generated in the second step of a two-step inorganic phototropic growth process depends on preexisting structure that has been first grown under different optical stimulation conditions. Se-Te generated with static illumination exhibited a highly anisotropic lamellar morphology with a characteristic feature pitch proportional to the input wavelength. Growth using first a short wavelength of light, followed by a growth using a longer wavelength, resulted in the second stage morphology exhibiting termination of lamellae formed during the first growth step. The lamellar pitch at the end of the second growth step was larger than that effected in the first step. In contrast, use of the same input wavelengths but in the opposite order produced no change in the feature pitch but rather only linear feature extension. Analysis of light absorption in the simulated structures, in tandem with the empirical data, indicated that the history effect and asymmetric path dependence are a result of emergent nanophotonic processes at the growth interface that dynamically shape the optical field and direct morphological evolution of the photodeposit in a continuous feedback loop.

Keywords: Electrochemistry, electrodeposition, photoelectrochemistry, nanoscale, nanostructure, mesostructure, semiconductor

Many living organisms exhibit phototropism wherein physical growth is directed to optimize collection of insolation.[1] Analogously, photoelectrochemical materials synthesis using polarized illumination can produce ordered, anisotropic lamellae that grow toward the incident light source.[2-4] Such inorganic phototropic growth produces spatially directed, ordered films using incoherent, unpatterned illumination of an optically isotropic nonphotoactive substrate in an optically isotropic solution.[5]

Biological systems that display phototropism can also exhibit adaptive morphologies in response to changes in environmental light conditions.[6] For inorganic phototropic growth, changes in the illumination wavelength produce changes in the lamellar period of the deposited material, and changes in the optical polarization yield lamellae oriented along the arbitrarily selected direction of polarization.[7,8] Multi-step inorganic phototropic growth, in which each step utilizes mutually different optical inputs, can effect three-dimensional structural complexity wherein the morphology varies along the growth direction reflecting the optical excitation present during each specific growth step. Herein we report observation of a path-dependent "history" effect in the multi-step inorganic phototropic growth of Se-Te alloys. The morphology of the photoelectrodeposit produced using a second input wavelength in a two-step growth process depends on the morphology of the mesoscale structure generated in the first growth stage. This history-effect phenomenon reflects the dynamic emergent nanophotonic behavior of the growing phototropic film, and is thus an intrinsic physical characteristic of inorganic phototropic growth, as opposed to a chemical or crystallographic bias of the growth process in the Se-Te material.[9,10]

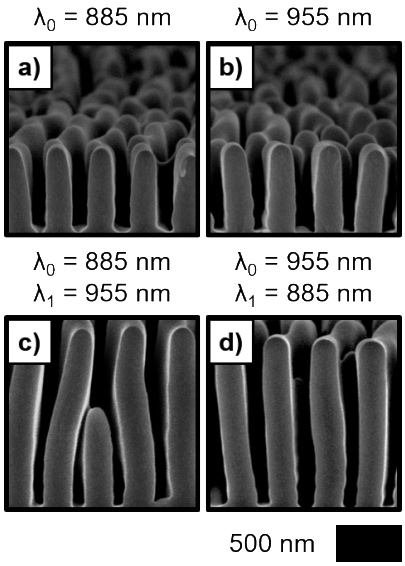

Figure 1. Representative cross-sectional SEMs of deposits generated with the indicated λ_0 illumination (a) and (b) and then extended with the indicated λ_1 illumination (c) and (d).

Polycrystalline Se-Te was photoelectrochemically grown from an acidic, aqueous solution of oxide precursors. Figure 1a,b present representative cross-sectional scanning-electron micrographs (SEMs) of deposits generated using linearly polarized and spatially uniform illumination from light-emitting diode (LED) sources with intensity-weighted average wavelengths, λ_{avg}, of 885 nm or 955 nm. Both deposits exhibited periodic, nanoscale lamellar features that projected outward from the substrate surface along the normal axis, with a high degree of out-of-plane anisotropy and similar feature heights (growth rate of ~ 800 nm C^{-1} cm^2). The feature width and pitch effected using λ_{avg} = 955 nm (Figure 1b) was greater than that for λ_{avg} = 885 nm (Figure 1a). Two-dimensional Fourier transform (2D FT) analysis of complementary top-down SEM data indicated that the morphological periods of the deposits were 332 ± 2 nm and 363 ± 2 nm for growths with λ_{avg} = 885 nm and 955 nm, respectively. These periods quantitively matched the expected spatial modulation of the optical field amplitude at the growth front by interfacial scattering of the illumination (additional details in the Supporting Information).[2] The out-of-plane feature height was a function of the charge density passed during growth (Figure S4).

Consistently, the observed deposit morphology did not change substantially when the illumination intensity was varied while still passing the same total charge density during growth (Figure S5).

Figure 1c presents a representative cross-sectional SEM of a deposit initially grown using $\lambda_{avg} = \lambda_0 = 885$ nm illumination and then extended using $\lambda_{avg} = \lambda_1 = 955$ nm (analogous lower magnification SEM presented in Figure S3a). This deposit exhibited a decrease along the substrate normal of the in-plane feature density, with a portion of features exhibiting a termination of growth. Features adjacent to such terminated growth sites were not spatially aligned solely along the surface normal, and some bent towards terminated features. 2D FT analysis yielded an interfacial feature pitch of 358 ± 10 nm, in accord with deposits generated using only $\lambda_{avg} = 955$ nm (Figure 1b). This behavior is consistent with prior results which indicate that each growth wavelength λ_{avg}, by itself produces a characteristic lamellar growth period.[7] The increase in period indicated by the 2D FT analysis suggests that 7 ± 3 % of lamellar features terminated, consistent with the termination rate of 9 ± 4 % obtained from inspection of cross-sectional SEM data. Additionally, 14 ± 8 % of the initial features exhibited bending, accommodating the new growth period in the two-step growth. The new in-plane periodic order evident in the cross-sectional data occurred when the preexisting deposit had extended 213 ± 82 nm in the out-of-plane direction.

Figure 1d presents a representative SEM of a deposit grown in a similar two-step manner as that presented in Figure 1c, but with the order reversed such that $\lambda_0 = 955$ nm and $\lambda_1 = 885$ nm (analogous lower magnification SEM presented in Figure S3b). The features increased in height during the second growth stage, but the resulting morphology was qualitatively similar to growth using only $\lambda_{avg} = 955$ nm (Figure 1b). No change in the in-plane feature density along the substrate normal was observed, and the interfacial period of 365 ± 2 nm quantitatively matched that observed for growth using only $\lambda_{avg} = 955$ nm. The growth was thus clearly path-dependent and

asymmetrically exhibited a history effect, with increases in the growth wavelength from 885 nm to 955 nm producing a change in feature density whereas no change was observed when the growth wavelength was instead decreased from 955 nm to 885 nm. Directed modulation of in-plane feature density may present utility for physical information storage. The morphology encodes the optical growth inputs, which could be varied and used to store an input data stream.

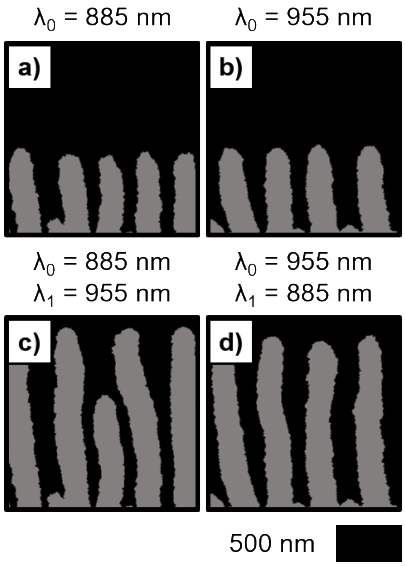

Figure 2. Simulated deposit morphologies generated with the indicated λ_0 illumination (a) and (b) and then extended with the indicated λ_1 illumination (c) and (d).

To gain insight into whether the path-dependent growth is an intrinsic consequence of asymmetric evolution of internal optical fields in the emerging, growing deposit, or potentially indicates a structural or chemical metastability, optically based computer simulations of the growth were performed. A two-step iterative model was utilized wherein electromagnetic simulations of light absorption were used to direct mass addition via a Monte Carlo method. Empirical inputs were limited to estimates of the complex refractive index of the deposits and the electrolyte index. The model contained only Maxwell's equations, with no chemical or structural bias towards selective morphology growth. Figure 2 shows that the simulated morphologies generated using optical inputs analogous to those used experimentally (Figure 1) closely reproduced the

experimental observations, confirming that the physical origin of the growth process asymmetry is ascribable to light-material interactions during growth.

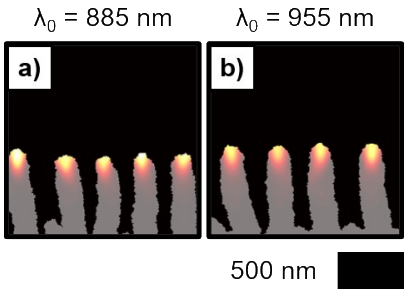

Figure 3. Simulated profiles of absorption of the indicated λ_0 illumination in deposit morphologies generated by growth modeling with the same λ_0.

Figure 3a and b present simulated profiles of light absorption in deposit morphologies generated via modeling using λ_{avg} = 885 nm and 955 nm, respectively, and illuminated with the same λ_{avg}. Both profiles exhibited concentrated absorption in the feature tips near the growth interface. Local enhancements in optical absorption result in local increases in mass deposition, so the simulated absorption concentration indicates that material addition should occur preferentially at the feature tips, resulting in linear feature extension. This modeled behavior is consistent with the morphological anisotropy and periodicity observed experimentally and indicates that growth can spontaneously produce a structure that optimizes interfacial optical concentration of the specific light input.

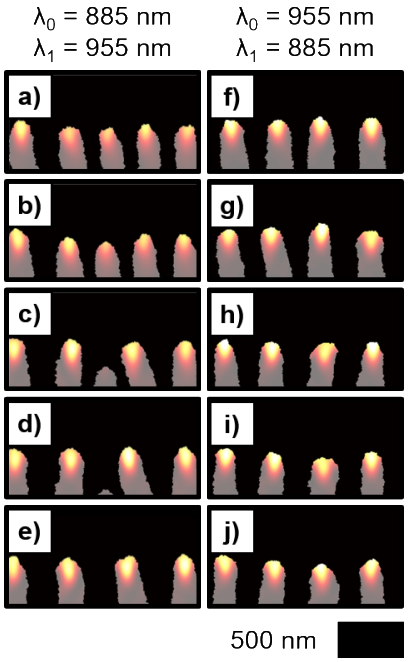

Figure 4. Simulated profiles of absorption of the indicated λ_1 illumination in deposit morphologies generated by growth modeling. In each column, panels from top to bottom present profiles for successive iterations of simulated morphologies generated initially using the indicated λ_0 illumination and progressively extended with the indicated λ_1 illumination.

Figure 4a-e presents successive simulated profiles of absorption of $\lambda_{avg} = \lambda_1 = 955$ nm during growth after initial structure generation using $\lambda_0 = 885$ (as in Figure 2c). A similar magnitude and concentration of absorption was present in all lamellar tips (Figure 4a), however, the centermost feature exhibited slightly decreased absorption and height relative to adjacent features (Figure 4b). The localized decrease in absorption resulted in local attenuation of growth, and thus the centermost feature grew less rapidly than adjacent features (Figure 4c). The decreased height resulted a self-reinforcing decrease in local absorption, with concomitant increased absorption in adjacent features and anisotropic localization of the absorption resonances in the tips of the adjacent features collectively stunting growth of the attenuated centermost feature. The asymmetric absorption also directed adjacent feature growth at an inclination from the substrate normal, towards the attenuated feature (Figure 4d). This morphological evolution further reduced the absorption in the centermost feature, leading to termination and an increased interfacial feature

pitch (Figure 4e). At this point, the resonances in the nearest neighbor features were localized more symmetrically in the tips, indicating linear growth extension with the new morphological period. The absorption behavior suggests that the growth process can evolve a deposit along the out-of-plane dimension to optimize the interfacial optical concentration in response to a change in input λ_{avg}. This evolution is a consequence of positive feedback, wherein regions coupling more effectively with the new optical input exhibit elevated rates of growth and increased light harvesting, as well as of negative feedback, wherein regions not coupling effectively exhibit decreased rates of growth, lessening parasitic absorption.

Figure 4f-j presents similar profiles of light absorption as in Figure 4a-e, but for absorption of $\lambda_{avg} = \lambda_1 = 885$ nm after initial growth using $\lambda_0 = 955$ nm (i.e. Figure 2d). Initially, all lamellar tips exhibited nearly identical magnitudes and degrees of concentration of optical absorption (Figure 4f). In each of the subsequent simulations (Figure 4g-j) the absorption intensity in certain features increased, but then regressed again in later simulations, and the opposite behavior was also observed. Simultaneously, in certain iterations the locations of specific absorption resonances deviated from the center of the feature tips, which led to transient growth at an inclination from the substrate normal. In later simulations the absorption concentration shifted to the opposite side of the same features, reversing the inclination and thereby resulting in net progressive growth normal to the substrate. These temporal oscillations in the absorption, both in magnitude and in spatial location, indicate that dynamic linear extension of the interfacial morphology defined by the initial optical input (λ_0) can sufficiently accommodate coupling with the new optical input (λ_1) in a manner that suppresses a change in the interfacial feature density. The path-dependent asymmetry in the morphological evolution in response to equal magnitude changes in the optical input (λ_{avg}) observed here is thus ascribable to the capacity of the initial structure, defined by $\lambda_0 =$

955 nm, to evolve linearly in response to λ_1 = 885 nm, with the greater feature width and pitch enabling dynamic accommodation of coupling to the shorter wavelength through oscillation of the absorption resonances. The finding that the path dependence observed experimentally also spontaneously emerged from the optically based growth modeling, provides strong support for the conclusion that the path-dependent structures do not represent chemically or kinetically metastable states nor reflect specific chemical or structural interactions. The observed behavior is instead a direct consequence of the interplay between light and matter that underpins inorganic phototropic growth: a dynamic, synergistic feedback loop wherein the growing material shapes the near-field optical profile, promoting and focusing subsequent mass deposition and thus responsively shaping the growing material.

In summary, a history effect was observed during inorganic phototropic growth wherein an initial mesostructure, defined by an initial input wavelength, influenced subsequent growth with a second, distinct input wavelength, to produce a different morphology in the second phase of growth than was produced via single-stage growth with this second input wavelength as the only input. This effect exhibited an asymmetric path dependence wherein discrete mesoscale structural evolution could be directed by the use of two sequential, discrete wavelength inputs, yet the use of the same inputs, but in the opposite order, resulted in only linear extension of the initial growth features. This path-dependent history effect is a result of the emergent nanophotonic phenomena directing light absorption dynamically during growth. Dynamic, metastable accommodation of a new optical input during growth suppressed mesostructural evolution. These results provide an impetus to explore the morphological response to a wide range of dynamic optical input modulations, and may consequently enable the generation of mesostructures with intricate three-dimensional complexity as well as defined interfacial optical coupling behavior.

SUPPORTING INFORMATION.

Additional details regarding experimental and computer modeling methods, additional scanning-electron micrographs, and additional computer simulation data.

AUTHOR INFORMATION.

*nslewis@caltech.edu

Notes

The authors declare no competing financial interest.

ACKNOWLEDGMENTS.

This work was supported by the "Light-Material Interactions in Energy Conversion" Energy Frontier Research Center funded by the U.S. Department of Energy, Office of Science, Office of Basic Energy Sciences under Award Number DE-SC0001293 and was also supported by the National Science Foundation, Directorate for Mathematical & Physical Sciences, Division of Materials Research under Award Number DMR 1905963. The authors gratefully acknowledge J. Thompson for insightful discussions, E. Simonoff and S. Yalamanchili for assistance with substrate preparation, and R. Gerhart, N. Hart, and B. Markowicz for assistance with photoelectrochemical cell fabrication. KRH and MCM acknowledge Graduate Research Fellowships from the National Science Foundation. MCM also acknowledges the Resnick Sustainability Institute at Caltech for fellowship support.

REFERENCES.

(1) Christie, J. M.; Murphy, A. S. Shoot phototropism in higher plants: New light through old concepts. *Am. J. Bot.* **2013**, *100*, 35-46.

(2) Carim, A. I.; Batara, N. A.; Premkumar, A.; Atwater, H. A.; Lewis, N. S. Polarization Control of Morphological Pattern Orientation During Light-Mediated Synthesis of Nanostructured Se-Te Films. *ACS Nano* **2016**, *10*, 102-111.

(3) Hamann, K. R.; Carim, A. I.; Meier, M. C.; Thompson, J. R.; Batara, N. A.; Yermolenko, I. S.; Atwater, H. A.; Lewis, N. S. Optically tunable mesoscale CdSe morphologies via inorganic phototropic growth. *J. Mater. Chem. C* **2020**, 12412-12417.

(4) Carim, A. I.; Hamann, K. R.; Batara, N. A.; Thompson, J. R.; Atwater, H. A.; Lewis, N. S. Template-Free Synthesis of Periodic Three-Dimensional PbSe Nanostructures via Photoelectrodeposition. *J. Am. Chem. Soc.* **2018**, *140*, 6536-6539.

(5) Meier, M. C.; Cheng, W.-H.; Atwater, H. A.; Lewis, N. S.; Carim, A. I. Inorganic Phototropism in Electrodeposition of Se-Te. *J. Am. Chem. Soc.* **2019**, *141*, 18658-18661.

(6) Hutchings, M. J.; de Kroon, H. Foraging in Plants: the Role of Morphological Plasticity in Resource Acquisition. In *Advances in Ecological Research*; Begon, M., Fitter, A. H., Eds.; Academic Press: London, 1994; Vol. 25, pp 159-238.

(7) Carim, A. I.; Batara, N. A.; Premkumar, A.; Atwater, H. A.; Lewis, N. S. Self-Optimizing Photoelectrochemical Growth of Nanopatterned Se-Te Films in Response to the Spectral Distribution of Incident Illumination. *Nano Lett.* **2015**, *15*, 7071-7076.

(8) Carim, A. I.; Batara, N. A.; Premkumar, A.; May, R.; Atwater, H. A.; Lewis, N. S. Morphological Expression of the Coherence and Relative Phase of Optical Inputs to the Photoelectrodeposition of Nanopatterned Se-Te Films. *Nano Lett.* **2016**, *16*, 2963-2968.

(9) Xiao, Z.-L.; Han, C. Y.; Kwok, W.-K.; Wang, H.-H.; Welp, U.; Wang, J.; Crabtree, G. W. Tuning the Architecture of Mesostructures by Electrodeposition. *J. Am. Chem. Soc.* **2004**, *126*, 2316-2317.

(10) Siegfried, M. J.; Choi, K.-S. Elucidating the Effect of Additives on the Growth and Stability of Cu_2O Surfaces via Shape Transformation of Pre-Grown Crystals. *J. Am. Chem. Soc.* **2006**, *128*, 10356-10357.

TABLE OF CONTENTS (TOC) GRAPHIC.

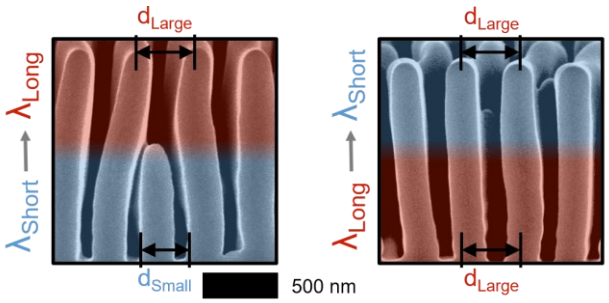

ASYMMETRIC OPTICAL GROWTH INSTRUCTION